Applied Physics Letters

Liquid crystal programmable metasurface for terahertz beam steering

Cite as: Appl. Phys. Lett. **116**, 131104 (2020); https://doi.org/10.1063/1.5144858
Submitted: 11 January 2020 . Accepted: 15 March 2020 . Published Online: 31 March 2020

Jingbo Wu, Ze Shen, Shijun Ge, Benwen Chen, Zhixiong Shen, Taofeng Wang, Caihong Zhang, Wei Hu, Kebin Fan, Willie Padilla, Yanqing Lu, Biaobing Jin, Jian Chen, and Peiheng Wu

Applied Physics Letters ARTICLE scitation.org/journal/apl

Liquid crystal programmable metasurface for terahertz beam steering

Cite as: Appl. Phys. Lett. **116**, 131104 (2020); doi: 10.1063/1.5144858
Submitted: 11 January 2020 · Accepted: 15 March 2020 ·
Published Online: 31 March 2020

View Online Export Citation CrossMark

Jingbo Wu,[1] Ze Shen,[1] Shijun Ge,[2] Benwen Chen,[1] Zhixiong Shen,[2] Taofeng Wang,[1] Caihong Zhang,[1] Wei Hu,[2] Kebin Fan,[3] Willie Padilla,[3] Yanqing Lu,[2,a)] Biaobing Jin,[1,b)] Jian Chen,[1] and Peiheng Wu[1]

AFFILIATIONS

[1]Research Institute of Superconductor Electronics (RISE), School of Electronic Science and Engineering, Nanjing University, 163 Xianlin Avenue, Nanjing 210023, China

[2]National Laboratory of Solid State Microstructures, Collaborative Innovation Center of Advanced Microstructures and College of Engineering and Applied Sciences, Nanjing University, 163 Xianlin Avenue, Nanjing 210023, China

[3]Department of Electrical and Computer Engineering, Duke University, Durham, North Carolina 27708, USA

[a)]Electronic address: yqlu@nju.edu.cn
[b)]Author to whom correspondence should be addressed: bbjin@nju.edu.cn

ABSTRACT

The coding metasurface integrated with tunable materials offers an attractive alternative to manipulate the THz beam dynamically. In this work, we demonstrate a THz programmable metasurface based on liquid crystal. The phase profile on the metasurface could be dynamically manipulated by switching the "0" and "1" states of each element. The programmable metasurface could deflect the THz beam using the designed coding sequence, and a maximum deflection angle of 32° has been achieved. The presented design opens a route of beamforming for THz communication.

The specific advantages of terahertz (THz) radiation have promised a great many applications such as wireless communication, medical imaging, homeland security, and astronomy.[1–4] THz communication has great opportunities in the upcoming 6G technology as it could deliver a high data rate of Tbit/s.[2] However, the serious attenuation of the THz wave in the atmosphere poses a challenge to THz communication. To overcome the issue of high propagation loss in the atmosphere, THz beamforming technology capable of directing the THz wave via the most efficient path dynamically is in great demand.[5] However, the phase shifters available at microwave frequencies are not effective at THz frequencies. The active THz beam steering techniques are still lacking.

Electromagnetic metamaterials (MMs) and metasurfaces offer us an effective way to manipulate the amplitude, phase, polarization, and orbital angular momentum of electromagnetic waves.[6–11] They have been widely used to develop THz functional devices toward the aforementioned applications.[12–16] For THz beamforming, it is important to manipulate the phase profile arbitrarily. The rise of coding and programmable metasurfaces greatly facilitates the phase manipulation by distributing binary coding elements on the surface and switching the coding state of each element dynamically.[17–22] Moreover, recent research combining the concept of coding metasurfaces with many other research fields such as information processing, holographic imaging, and artificial intelligence greatly extended the scope of metasurfaces.[23–28]

In order to develop programmable metasurfaces to manipulate the phase of the THz wave, the tunable components at THz frequencies are essential. The semiconductor lumped components widely used in microwave programmable metasurfaces hardly work in the THz band. In previous studies, integrating the tunable materials such as graphene, liquid crystals (LCs), and phase-change materials into metasurfaces has been proven to be a viable way for dynamic THz modulation.[29–36] Due to the birefringence effect of LCs, the phase retardation can be altered by switching the orientation of the LC molecules dynamically.[37–43] The tunable phase shift of LC devices enabled the dynamic control of THz beam deflection.[39–41,43] Furthermore, similar to the LC display technology, the LC-based MM can be pixilated, and each pixel can be electrically addressable.

In this work, we propose a THz programmable metasurface capable of beam steering. By embedding the tunable LC layer into the metamaterial absorber, we could achieve a phase change of π electrically for each element in the one-dimensional array. When different coding sequences were applied on the array, the phase profile on the surface could be changed and the reflected THz beam would deflect an angle correspondingly. We envision that our work offers an avenue for active and intelligent beamforming toward potential applications.

The sketch of the proposed programmable metasurface array is shown in Fig. 1. It consists of a 24-element linear array, and each element is composed of 50 rows and 2 columns of unit cells. The unit cell has a metal-insulator-metal (MIM) resonator structure. It could provide a reflective phase change of 2π when the resonator works in the overcoupled regime, i.e., the radiative loss is larger than the absorption loss.[30,43] The top and bottom metallic layers have the patterns of Jerusalem cross and pixelated rectangle patch, respectively. They are both fabricated onto 500-μm-thick silicon dioxide substrates. The metallic layers together with their substrates and the supporting Mylar film form the LC cell. The thickness of the LC layer is 25 μm. LC NJU-LDN-4 is filled into the cell, and its birefringence is about 0.3 at THz frequencies.[44] The alignment layers are spin-coated onto the two metallic layers to keep the orientation direction of LC molecules.

When the electric field is applied between the two metallic layers, the LC molecules reorient and the refractive index of the LC layer changes correspondingly. As a result, the absorption frequency of the metamaterial absorber shifts with the change in the refractive index of the LC layer. In that case, the reflection amplitude and phase can be modulated by the electric field. By carefully choosing the bias voltage, we can obtain two states with the same reflection amplitude and a relative phase difference of π. The two states are defined as 0 and 1 states for coding metamaterials. In this work, a square wave signal with a frequency of 100 Hz was used for bias, and the actual bias voltages for 0 and 1 were 0 and 40 V, respectively. To realize the THz beam steering with this LC metasurface, we use an FPGA board to generate the coding sequences. The coding sequence signals output from FPGA are amplified by a 24-channel amplifier circuit, and each channel is in connection with an element of the linear array. Thus, we can electrically address each element of the linear array independently.

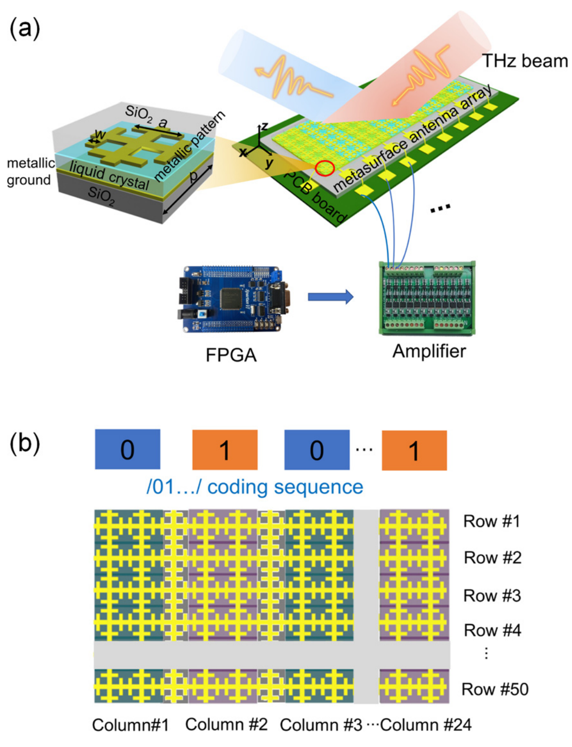

FIG. 1. The schematic of the THz programmable metasurface. (a) The 3D view of the THz programmable metasurface and control circuits. The metasurface consists of a 24-element linear array, and each element is in connection with a multi-channel amplifier. The FPGA outputs control signals, and the amplified signals are used to control the phase of every element individually. The unit cell consisting of an LC layer embedded into two metallic layers is shown in the left inset, where $p = 170\ \mu$m, $a = 86\ \mu$m, and $w = 20\ \mu$m. (b) The planar graph of the programmable metasurface (bottom) and the applied coding sequence of /01…/ (top).

Figures 2(a) and 2(b) show three different states about the distribution of the LC molecule orientation and the simulated reflection spectra. Ideally, in response to the bias voltage, all the LC molecules in the cell will reorient from the pre-aligned horizontal direction (state *a*) to the vertical direction (state *b*). In that case, the dielectric constant of the LC changes from the extraordinary refractive index (n_e) to the ordinary refractive index (n_o). In the simulation, the refractive index of the LC is set as $n_e = 1.57$ and $n_o = 1.87$ according to the results of LC NJU-LDN-4 measured at THz frequencies.[44] The difference of the refractive index gives rise to a large frequency shift from 683 GHz to 633 GHz, and the maximum phase delay between two states is almost 2π as shown in Fig. 2(b). Due to the low filling factor of the top metallic layer, the distribution of the LC molecule orientation is inhomogeneous. When the biased voltage is applied, only the LC molecules in the region underneath the metallic part will reorient, while the others remain in the horizontal orientation. This case is shown as state *c* in Fig. 2(a). As a result, the equivalent refractive index of the inhomogeneous LC layer takes a value between n_e and n_o. If we take the filling factor of the top metallic layer into account and suppose that half of LC molecules in the metallic region could reorient, the equivalent

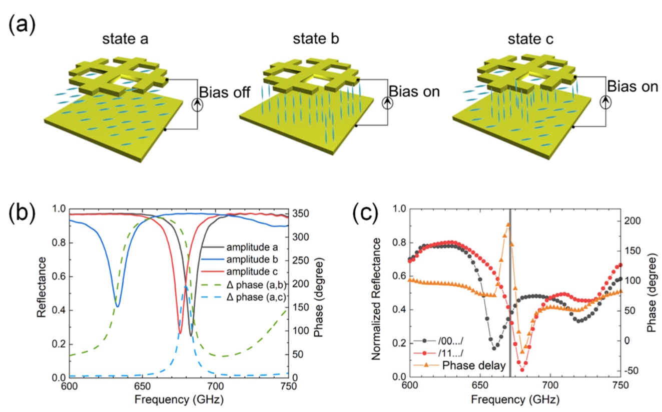

FIG. 2. (a) The diagram of LC alignment when the voltage is applied between two metallic layers in a unit cell. There is no applied bias, and all the LC molecules are aligned along the horizontal direction in state *a*. The applied bias is on, and all the LC molecules are aligned along the electric field direction in state *b*. The applied bias is on, and only a portion of LC molecules is aligned along the electric field direction in state c. (b) The simulated reflection spectra of the metasurface in three different states and the corresponding phase delay between two states. (c) The measured frequency response of the programmable metasurface when all the elements are in "0" or "1" states and their phase delay. The working frequency of 672 GHz is indicated by a gray reference line.

refractive index is set to be 1.63 in state *c*. In Fig. 2(b), the frequency shift and the maximum phase delay from state *a* to state *c* are much smaller those from state *a* to state *b*. We note that the maximum phase delay at 670 GHz is near π, and the reflection coefficient at the frequency is almost the same, which satisfies the requirement of 0 and 1 elements for the 1-bit coding metasurface.[17]

Figure 2(c) shows the measured results of the fabricated metasurface sample when all the array elements are unbiased (denoted by the /00…/ sequence) and biased (denoted by the /11…/ sequence) using the THz time-domain spectroscopy (TDS) system. As displayed in Fig. 2(c), there is an obvious frequency shift for the two states. The measured results at /11…/ and /00…/ sequences are in good accordance with the simulated results of state *c* and state *a*, respectively. At 672 GHz (gray reference line), the reflectance coefficient at /11…/ and /00…/ sequences is almost equal. Moreover, the phase delay of these two sequences at that frequency is about 190°.

In order to evaluate whether the complex reflectance satisfies the requirement of 0 and 1 elements for the 1-bit coding metasurface or not, we define a parameter called the binary bit reflectance ratio (BBRR)

$$\mathrm{BBRR} = \left|\frac{\Gamma_0 - \Gamma_1}{\Gamma_0 + \Gamma_1}\right|, \tag{1}$$

where Γ_0 and Γ_1 are the complex reflectances at two states. Indeed, the BBRR is the ratio of the modulus of the difference between Γ_0 and Γ_1 to the modulus of their sum. Ideally, Γ_0 and Γ_1 should have the same amplitude and a phase difference of π, so their sum is zero and the BBRR is infinite. In the actual case, the sum of Γ_0 and Γ_1 corresponds to the component of unwanted specular reflection. The higher the BBRR, the higher the efficiency of beam deflection. If the BBRR is 5, 83% of energy will be deflected. Therefore, the BBRR of over 5 is thought to be acceptable for THz beam deflection. In our measurement, the BBRR reaches to a peak value of 7 at 672 GHz. It means that the proposed unit cell with proper electric bias is well suited for the 1-bit coding metasurface.

If we apply the coding sequence onto the 24-element linear array, the phase profile can be changed. Based on the general Snell's law and phased array theory, the reflected beam can deflect an angle, which depends on the phase gradient introduced by the coding pattern.[8,29] The deflection angle (θ_s) can be expressed as

$$|\sin\theta_s - \sin\theta_0| = \frac{\lambda}{\mathrm{Md}}, \tag{2}$$

where θ_0 is the specular reflection angle, λ is the operating wavelength, *d* is the distance of the element in the linear array, and *M* corresponds to the number of elements in a subarray. According to Eq. (2), if we change the periodicity of the subarray, the deflection angle of the THz beam can be tuned.

Then, we measured the THz beam deflection capability of this programmable metasurface. The optical fiber-based THz TDS system was used to measure the angular distribution of the deflected THz beam. The sample was fixed at the center of the rotation stage. The THz emitter and receiver modules were fixed at the ends of two arms in the rotation stage. The THz beam excited from the emitter was incident at 20° and TM polarized. The THz signals at different angles were collected by the receiver by rotating the corresponding arm. After calculating the Fourier transform of the received signals at each angle, we could obtain the angular distribution of the deflected THz beam. The reflected power distributions are normalized to the reflection amplitude of the gold mirror. Therefore, the values correspond to the deflection efficiency.

Figure 3 shows the measured reflected beam distribution at 672 GHz for the applied five coding sequences. The applied coding sequences are /00…/, /11…/, /10…/, /1100…/, and /111000…/, respectively. When we switch the coding sequences, the variance of the periodicity of the subarray results in a change in the deflection angle. The calculated maximum beam deflection angle for the sequences of /10…/, /1100…/, and /111000…/ and the experimental results are listed in Table I. As can be seen, the difference between the measured and calculated results is within 1°, indicating that our proposed metasurface can achieve beam deflection as we design. In our present design, since the minimum value of M is 2, the maximum deflection angle is 31.2°. The maximum deflection angle could be increased by decreasing the spacing of elements in the linear array. The angular spread of the deflected beam is about 5°. If the number of elements is increased, the deflected beams will become narrower.

As shown in Fig. 3, the deflection efficiency for coding sequences of /10…/, /1100…/, and /111000…/ are 19.1%, 20.4%, and 21.3%, respectively. For comparison, we calculated the angular distribution with different coding sequences based on the beam steering theory

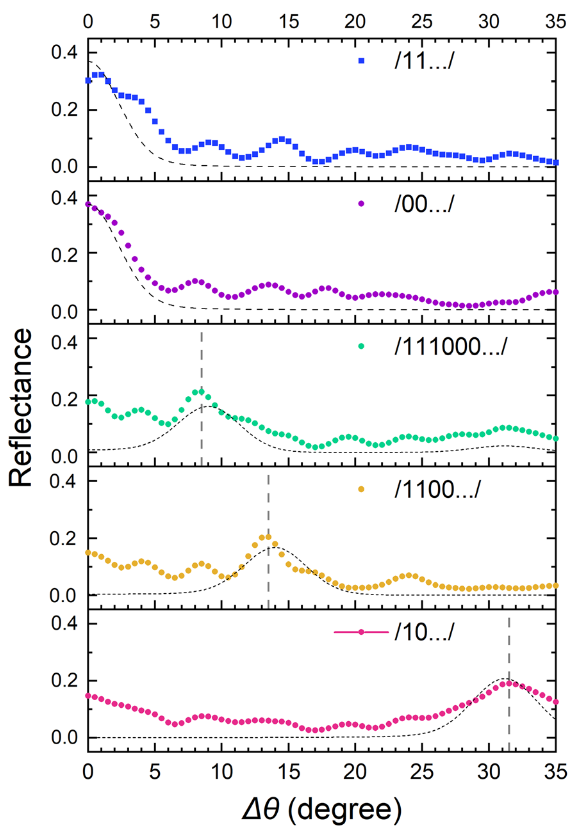

FIG. 3. The measured (dots) and calculated (dashed lines) angle distributions of the reflected beam at 672 GHz for five different coding sequences with an incident angle of 20°, and $\Delta\theta$ is the angle relative to the specular angle.

TABLE I. The measured beam deflection angles at 672 GHz with three different coding sequences and the corresponding calculated results based on Eq. (2).

Coding pattern	Calculated θ_s	Measured θ_s
/10…/ (M = 2)	31.2°	31.5°
/1100…/ (M = 4)	14.1°	13.5°
/111000…/ (M = 6)	9.2°	8.5°

and the measured reflection efficiency of the metasurface element. The calculated results (dashed lines) in Fig. 3 show good agreement with the experimental results. We noticed that the specular reflection is still evident. It is mainly attributed to the nonuniformity and the low BBRR of elements in the linear array.

In our experiment, we found that the beam steering capability degrades a lot when the frequency is away from the optimal frequency of 672 GHz. It suggests that the beam steering capability is greatly relevant to the BBRR. We also measured the beam deflection with different coding sequences with the incident angles of 40° and 60°, and the beam steering capability becomes much worse. The low efficiency at large incident angles is mainly because the radiation gain of a single element drops a lot according to our simulation results.

The efficiency of beam deflection is still not as high as we expect. It can be attributed to the following reasons: At first, the reflection efficiency of the element in the linear array is still low. At the working frequency of 672 GHz, the reflection amplitude for the /11…/ and /00…/ sequences is below 0.4. It means that more than 60% of energy is absorbed rather than being reflected. Based on recent works, the THz reflector array with high reflectance and a tuning range of over π could be obtained using the MIM resonator when the radiative loss is much larger than the absorption loss.[30,43,45] By optimizing the design of the MIM resonator and choosing the LC with lower absorption loss, the deflection efficiency could be greatly improved.[42,43] Second, the 1-bit coding metasurface has a relatively low deflection efficiency as the beam is deflected into the +1 and −1 order equally.[17] In this work, the maximum phase shift is about π, and we adopted the design of the 1-bit coding metasurface. If we could realize a phase tuning range of 2π, we could develop 2-bit or 3-bit coding LC metasurfaces and obtain higher beam deflection efficiency.[17–19,43] Choosing the metasurface geometry with a higher filling factor is a viable way to expand the phase tuning range because more LC molecules could reorient with the applied electric field. Third, the presence of specular reflection degrades the deflection efficiency. Increasing the BBRR of each element and improving its uniformity will be beneficial for the increase in beam deflection efficiency.

In this study, we demonstrate a THz programmable linear array based on the LC metasurface, which can manipulate the phase distribution dynamically. We realize the control of beam deflection by changing the coding sequences, and the deflection angle is as large as 32°. The beam steering efficiency and working bandwidth can be further improved by optimizing the design of the metasurface. Our design can be extended to a two-dimensional pixelated THz metasurface, offering a promising solution of dynamic beam steering and beamforming at THz frequencies. The LC-based programmable metasurface could enable the broad adoption of THz wireless communication, computational imaging, and target identification.

See the supplementary material for beam steering theory and the device fabrication process.

AUTHOR'S CONTRIBUTIONS

J.W. and Z.S. contributed equally to this work.

This work was supported by the National Key Research and Development Program of China (No. 2017YFA0700202), the National Nature Science Foundation of China (NSFC) (Nos. 61521001, 61731010, and 61701219), the Jiangsu Provincial Natural Science Fund (No. BK20170649), the Fundamental Research Funds for the Central Universities, and the Research Fund for Jiangsu Key Laboratory of Advanced Techniques for Manipulating Electromagnetic Waves.

REFERENCES

1M. Tonouchi, Nat. Photonics **1**, 97 (2007).
2T. Nagatsuma, G. Ducournau, and C. C. Renaud, Nat. Photonics **10**, 371 (2016).
3W. L. Chan, J. Deibel, and D. M. Mittleman, Rep. Prog. Phys. **70**, 1325 (2007).
4F. Sizov and A. Rogalski, Prog. Quantum Electron. **34**, 278 (2010).
5X. Fu, F. Yang, C. Liu, X. Wu, and T. J. Cui, Adv. Opt. Mater. **8**, 1900628 (2019).
6D. R. Smith, Science **305**, 788 (2004).
7J. B. Pendry, Science **312**, 1780 (2006).
8N. Yu, P. Genevet, M. A. Kats, F. Aieta, J.-P. Tetienne, F. Capasso, and Z. Gaburro, Science **334**, 333 (2011).
9N. A. Rubin, G. D'Aversa, P. Chevalier, Z. Shi, W. T. Chen, and F. Capasso, Science **365**, eaax1839 (2019).
10Q. He, S. Sun, S. Xiao, and L. Zhou, Adv. Opt. Mater. **6**, 1800415 (2018).
11N. Yu and F. Capasso, Nat. Mater. **13**, 139 (2014).
12H.-T. Chen, W. J. Padilla, J. M. O. Zide, A. C. Gossard, A. J. Taylor, and R. D. Averitt, Nature **444**, 597 (2006).
13P. Conversion, N. K. Grady, J. E. Heyes, D. R. Chowdhury, Y. Zeng, M. T. Reiten, A. K. Azad, A. J. Taylor, D. A. R. Dalvit, and H. Chen, Science **340**, 1304 (2013).
14C. M. Watts, D. Shrekenhamer, J. Montoya, G. Lipworth, J. Hunt, T. Sleasman, S. Krishna, D. R. Smith, and W. J. Padilla, Nat. Photonics **8**, 605 (2014).
15H. Tao, C. M. Bingham, A. C. Strikwerda, D. Pilon, D. Shrekenhamer, N. I. Landy, K. Fan, X. Zhang, W. J. Padilla, and R. D. Averitt, Phys. Rev. B. **78**, 241103(R) (2008).
16J. Gu, R. Singh, X. Liu, X. Zhang, Y. Ma, S. Zhang, S. A. Maier, Z. Tian, A. K. Azad, H. Chen, A. J. Taylor, J. Han, and W. Zhang, Nat. Commun. **3**, 1151 (2012).
17T. J. Cui, M. Q. Qi, X. Wan, J. Zhao, and Q. Cheng, Light Sci. Appl. **3**, e218 (2014).
18S. Liu and T. J. Cui, IEEE J. Sel. Top. Quantum Electron. **23**, 4700312 (2017).
19L.-H. Gao, Q. Cheng, J. Yang, S.-J. Ma, J. Zhao, S. Liu, H.-B. Chen, Q. He, W.-X. Jiang, H.-F. Ma, Q.-Y. Wen, L.-J. Liang, B.-B. Jin, W.-W. Liu, L. Zhou, J.-Q. Yao, P.-H. Wu, and T.-J. Cui, Light Sci. Appl. **4**, e324 (2015).
20S. Liu, T. J. Cui, Q. Xu, D. Bao, L. Du, X. Wan, W. X. Tang, C. Ouyang, X. Y. Zhou, H. Yuan, H. F. Ma, W. X. Jiang, J. Han, W. Zhang, and Q. Cheng, Light Sci. Appl. **5**, e16076 (2016).
21S. Liu, T. J. Cui, L. Zhang, Q. Xu, Q. Wang, X. Wan, J. Q. Gu, W. X. Tang, M. Qing Qi, J. G. Han, W. L. Zhang, X. Y. Zhou, and Q. Cheng, Adv. Sci. **3**, 1600156 (2016).
22L. Zhang, X. Q. Chen, S. Liu, Q. Zhang, J. Zhao, J. Y. Dai, G. D. Bai, X. Wan, Q. Cheng, G. Castaldi, V. Galdi, and T. J. Cui, Nat. Commun. **9**, 4334 (2018).
23T.-J. Cui, S. Liu, and L.-L. Li, Light Sci. Appl. **5**, e16172 (2016).
24J. Zhao, X. Yang, J. Y. Dai, Q. Cheng, X. Li, N. H. Qi, J. C. Ke, G. D. Bai, S. Liu, S. Jin, A. Alù, and T. J. Cui, Natl. Sci. Rev. **6**, 231 (2019).
25L. Li, H. Ruan, C. Liu, Y. Li, Y. Shuang, A. Alù, C.-W. Qiu, and T. J. Cui, Nat. Commun. **10**, 1082 (2019).
26L. Li, Y. Shuang, Q. Ma, H. Li, H. Zhao, M. Wei, C. Liu, C. Hao, C.-W. Qiu, and T. J. Cui, Light Sci. Appl. **8**, 97 (2019).

[27] L. Li, T. Jun Cui, W. Ji, S. Liu, J. Ding, X. Wan, Y. Bo Li, M. Jiang, C.-W. Qiu, and S. Zhang, Nat. Commun. **8**, 197 (2017).
[28] Q. Ma, G. D. Bai, H. B. Jing, C. Yang, L. Li, and T. J. Cui, Light Sci. Appl. **8**, 98 (2019).
[29] M. Tamagnone, S. Capdevila, A. Lombardo, J. Wu, A. Centeno, A. Zurutuza, A. M. Ionescu, A. C. Ferrari, and J. R. Mosig, arXiv:1806.02202 (2018).
[30] Z. Miao, Q. Wu, X. Li, Q. He, K. Ding, Z. An, Y. Zhang, and L. Zhou, Phys. Rev. X **5**, 041027 (2015).
[31] P. Q. Liu, I. J. Luxmoore, S. A. Mikhailov, N. A. Savostianova, F. Valmorra, J. Faist, and G. R. Nash, Nat. Commun. **6**, 8969 (2015).
[32] S. Savo, D. Shrekenhamer, and W. J. Padilla, Adv. Opt. Mater. **2**, 275 (2014).
[33] Z. Shen, S. Zhou, S. Ge, W. Duan, P. Chen, L. Wang, W. Hu, and Y. Lu, Opt. Lett. **43**, 4695 (2018).
[34] G. Zhou, P. Dai, J. Wu, B. Jin, Q. Wen, G. Zhu, Z. Shen, C. Zhang, L. Kang, W. Xu, J. Chen, and P. Wu, Opt. Express **25**, 17322 (2017).
[35] P. Pitchappa, A. Kumar, S. Prakash, H. Jani, T. Venkatesan, and R. Singh, Adv. Mater. **31**, 1808157 (2019).
[36] C. Li, J. Wu, S. Jiang, R. Su, C. Zhang, C. Jiang, G. Zhou, B. Jin, L. Kang, W. Xu, J. Chen, and P. Wu, Appl. Phys. Lett. **111**, 092601 (2017).
[37] S. Li, X. Xu, R. Maruthiyodan Veetil, V. Valuckas, R. Paniagua-Domínguez, and A. I. Kuznetsov, Science **364**, 1087 (2019).
[38] L. Wang, S. Ge, W. Hu, M. Nakajima, and Y. Lu, Opt. Mater. Express **7**, 2023 (2017).
[39] C.-J. Lin, Y.-T. Li, C.-F. Hsieh, R.-P. Pan, and C.-L. Pan, Opt. Express **16**, 2995 (2008).
[40] C.-J. Lin, C.-H. Lin, Y.-T. Li, R.-P. Pan, and C.-L. Pan, IEEE Photonics Technol. Lett. **21**, 730 (2009).
[41] C.-L. Pan, C.-J. Lin, C.-S. Yang, W.-T. Wu, and R.-P. Pan, in *Liquid Crystals-Recent Advancements in Fundamental and Device Technologies*, edited by P. K. Choudhury (IntechOpen, 2018).
[42] G. Isić, B. Vasić, D. C. Zografopoulos, R. Beccherelli, and R. Gajić, Phys. Rev. Appl. **3**, 064007 (2015).
[43] B. Vasic, G. Isic, R. Beccherelli, and D. C. Zografopoulos, IEEE J. Sel. Top. Quantum Electron. **26**, 7701609 (2020).
[44] L. Wang, X. Lin, X. Liang, J. Wu, W. Hu, Z. Zheng, B. Jin, Y. Qin, and Y. Lu, Opt. Mater. Express **2**, 1314 (2012).
[45] D. Headland, T. Niu, E. Carrasco, D. Abbott, S. Sriram, M. Bhaskaran, C. Fumeaux, and W. Withayachumnankul, IEEE J. Sel. Top. Quantum Electron. **23**, 8500918 (2017).